Presented at the Yamada μSR Conference,
Shimoda, Japan, April 1983

LBL--16889

DE84 005196

SEARCH FOR RIGHT-HANDED CURRENTS IN MUON DECAY

J. Carr, G. Gidal, B. Gobbi†, A. Jodidio, C.J. Oram††,
K.A. Shinsky, H.M. Steiner, D. Stoker, M. Strovink, and R.D. Tripp

Lawrence Berkeley Laboratory and Department of Physics
University of California, Berkeley, California 94720

†Department of Physics, Northwestern University, Evanston, Illinois 60201

††Tri-University Meson Facility, Vancouver, BC, V6T2A3, Canada

ABSTRACT

We report new limits on right-handed currents, based on precise measurement of the endpoint of the e^+ spectrum from μ^+ decay. Highly polarized μ^+ from the TRIUMF "surface" beam were stopped in pure metal foils within either an 1.1-T spin-holding longitudinal field, or a 70-gauss spin-precessing transverse field. Decay e^+ emitted within 200 mrad of the beam direction were momentum-analyzed to ±0.2%. For the spin-held data, decay via (V-A) currents requires the e^+ rate to approach zero in the beam direction at the endpoint. Measurement of this rate sets the 90%-confidence limits $\xi P_\mu \delta/\rho > 0.9959$ and $M(W_R) > 380$ GeV, where W_R is the possible right-handed gauge boson. For the spin-precessed data we independently determine a 90% confidence limit $\xi P_\mu \delta/\rho > 0.9918$.

DISCLAIMER

Within the remarkably successful Glashow-Weinberg-Salam electroweak model[1], spontaneously broken gauge symmetry gives the left-handed gauge boson W_L a mass specified only as a function of the experimentally observed Fermi coupling strength. If the $U(1) \times SU(2)_L$ gauge group is extended e.g. to $U(1) \times SU(2)_L \times SU(2)_R$,[2] left-right symmetry at the Lagrangian level is restored with the addition of a right-handed gauge boson W_R. The dominance of left-handed charged currents at present energies could then arise from a W_L–W_R mass splitting which is tiny on the grand-unification scale.

In these left-right symmetric theories, the physical bosons W_1 and W_2, with mass-squared ratio $\alpha = M^2(W_1)/M^2(W_2)$, are linear combinations of the gauge bosons:

$$W_1 = W_L \cos\zeta - W_R \sin\zeta$$

$$W_2 = W_L \sin\zeta + W_R \cos\zeta$$

The effects of W_L–W_R mixing and W_2 exchange relative to W_1 exchange are independent of momentum transfer well below $M^2(W_1)$.[3,4] If the ν_R is light enough to be produced without significant kinematic effect, the strongest experimental limits[5-10] on α and the mixing angle ζ thus are obtained from muon and nucleon β decay. Additional constraints are placed by model-dependent calculations of the K_L–K_S mass difference[11,12] and of current-algebra relations between $K \to 3\pi$ and $K \to 2\pi$ amplitudes.[13] Present experimental bounds are displayed as contours in Fig. 1. To improve the experimental sensitivity, we have measured precisely the high-momentum region of the positron spectrum in polarized μ^+ decay. This letter presents new limits set by these data, represented in Fig. 1 by the small bold ellipse.

The stopped μ^+ decays of interest are those which emit e^+ near the momentum spectrum endpoint $x = p_e/p_e(max) = 1$, and also near $\theta = 0$, where π–θ is the angle between $\vec{p}_e$ and the direction of μ^+ polarization P_μ. Relative to that for unpolarized muons, the decay rate is

$$R(x,\theta) = 1 - \frac{1-2\bar{x}-\bar{\delta}+4\bar{x}\bar{\delta}}{1+2\bar{x}-\bar{\rho}+4\bar{x}\bar{\rho}}\,\xi P_\mu \cos\theta \quad , \qquad (1)$$

where $\bar{x} = 1-x$, $\bar{\delta} = 1-4\delta/3$, $\bar{\rho} = 1-4\rho/3$, and ξ, δ, and ρ are the usual muon decay parameters.[14] (Radiative corrections[15] and the finite electron mass are included in the actual analysis but neglected in (1) above.) At the endpoint, $R(1,0) = 1 - \xi P_\mu \delta/\rho$; and in the $(V-A)$ limit, $R(x\to1,\theta\to0) \approx 6-4x-P_\mu\cos\theta$. For a μ^+ beam derived from π^+ decay at rest, θ becomes the angle between the e^+ and μ^+ momenta. Then, in left-right symmetric theories,[3] $P_\mu \approx 1-2(\alpha+\zeta)^2$, and the endpoint decay rate $R(1,0) \approx 2(2\alpha^2 + 2\alpha\zeta + \zeta^2)$ constrains both α and ζ.

This experiment is made possible by the nearly complete μ^+ polarization of a beam derived from π^+ decay near the surface of the production target.[16] The M13 beam[17] at the Tri-University Meson Facility (TRIUMF) cyclotron is produced by π^+ decay within a bare 2 mm C target at 135° to the 520-MeV proton beam direction. The 29.5-MeV/c μ^+ are transported in vacuum through two 60° bends and are momentum-selected by slits at two intermediate foci. For collection of the present data, the beam angular acceptance was set to 20 msr, and the momentum acceptance typically to 1% FWHM, yielding 15,000 μ^+/sec into a 12 × 10 *mm* spot. A comparable flux of beam positrons is cut out by a stopping requirement at the muon target. The 2% contamination of prompt ("cloud") μ^+ from π^+ decay in flight is rejected by requiring the μ^+ to be produced well within the 43-nsec interval between proton bursts.

Details of the muon polarimeter and its trigger are shown in Fig. 2. After passing through 25 mg/cm^2 of low-Z material, beam μ^+ are measured with an angular resolution of 20 mrad. Target foils of 99.99% pure Al, Cu, Ag, and Au were chosen for their high concentrations of free electrons. The electron sea effectively prevents the depolarization which otherwise would result from muonium formation. With the help of *in situ* range measurements, the foil thicknesses (Table I) were selected to minimize μ^+ punch-through and decay e^+ scattering. A 1.1-T longitudinal field ($B_{||}$) is also applied to preserve the stopped μ^+ spin direction. During alternate hours the longitudinal field is nulled to within ±3 gauss and a 70-gauss transverse field ($B_\perp$) is substituted. This precesses the μ^+ spin about a vertical axis so that its time-average polarization is zero. Downstream of the target, the decay e^+ is measured with an angular resolution of 10 mrad and focussed by a 0.5 T-m solenoidal field lens. The septum between the target and solenoid bore makes the focal length nearly independent of the choice of field orientation at the target.

The decay e^+ is momentum-analyzed by a vertical dipole magnet having approximate cylindrical symmetry, producing a central field of 0.32 T. Driftchamber systems using methane-8% methylal gas are located at its conjugate foci, and the intervening volume is evacuated. The dispersion $\Delta p/p$ was measured to be 1.07%/cm by passing a positron beam through the spectrometer. All dipoles are NMR-controlled. In combination, the field lens and positron spectrometer accept 250 msr within a momentum bite of $\pm 20\%$; in the analysis described below, their acceptance and momentum bite were restricted to 160 msr and $\pm 8\%$.

The trigger requires the signature of a beam particle stopping in the foil target, in delayed (0.2 - 10 μsec) coincidence with the signature of a decay positron passing through the spectrometer. The central momentum accepted by the spectrometer is set near the decay spectrum endpoint (180% of the beam momentum). When the μ^+ component is removed from the beam, the raw trigger rate essentially vanishes. Events with an extra particle arriving in the target between the μ^+ stop and the decay time are tagged and rejected in the analysis.

The data reported here are based upon 3.5×10^6 triggers collected during an initial three-week run in 1982. An additional 10^7 triggers collected in late 1982 are presently being analyzed. During hourly tape changes, typically either the muon stopping foil or the field direction at the stopping point ($B_{||}$ or $B_{\perp}$) were changed; the spectrometer dipole was powered continuously. The standard TRIUMF data acquisition system logged events at rates above 100 Hz while introducing negligible deadtime; on-line analysis supplied physics as well as hardware diagnostic information, including the endpoint edge for $B_{\perp}$ data. In many special runs the beam momentum was moved above and well below the "surface edge", and other conditions were varied.

With allowance for local curvature, straight e^+ track segments were found separately in the horizontal and vertical projections of three groups of wire chamber planes; (P3, D1, D2); D3; and D4 (Fig. 2). All possible combinations of hits were considered and tracks in all six segments were found in 99% of the triggers. Of these, 95% had hit multiplicities which corresponded to a single incoming and outgoing track with little noise. The remainder were rejected to avoid possible confusion. Taking account of the magnetic fields, projections of track segments were required to agree at

the target, in the bore of the solenoid, and in position and vertical slope in the dipole. The trigger counter S3 provided an additional coarse position measurement, which was required to agree with that in D4.

Initially the nonlinear space-time relationships in the driftchambers were approximated using uniform-illumination data. Separately for each chamber and for each run, they were dynamically fine-tuned by minimizing residuals in the track-segment fits. Residuals of $\leq 500\ \mu$ were achieved in P3, D1, and D2; and $\leq 250\ \mu$ in the spectrometer chambers D3 and D4. The hits found in P1 through D2 were then fitted to curved trajectories based on the first-order optics of cylindrically symmetric fields.[18] The μ^+ and e^+ polar angles θ_μ and θ_e with respect to the beam axis at the target were thereby determined. Monte Carlo simulation based on higher-order field optics has verified the accuracy of this procedure to within an uncertainty in $\cos\theta$ of 0.0003. For the $B_{||}$ data the transverse component of the μ^+ spin precesses about the beam axis too rapidly to be followed. Thus for $\cos\theta = \hat{P}_\mu \hat{P}_e$ in Equation(1), we substitute $\cos\theta_\mu \cos\theta_e$, which is equivalent to an average over many events.

The e^+ momentum was obtained by taking the sum of the horizontal coordinates at the conjugate foci of the spectrometer magnet. Using the initially fit momentum, the average square deviation from the median plane, and the average impact parameter with respect to the magnet axis as parameters, this sum was empirically corrected to second order, based on the endpoint position in $B_\perp$ data and on data from special calibration runs. The sharp edge at $x = 1$ in Fig. 3(a) corresponds to a gaussian component of the positron momentum resolution which is less than 0.2%. The slightly rounded shoulder is due primarily to Bhabha straggling in the 180 mg/cm^2 of material upstream of the spectrometer vacuum.

In addition to cuts on μ^+ time of production, track ambiguity, and track linkage described above, conservative fiducial cuts were applied, and events with $x < 0.92$ and $\cos\theta < 0.975$ were dropped from the analysis. The final x distributions in Fig. 3 preserve 7.5% of the triggers. This rate of survival is the result of loose triggering and generous acceptance, with tight cuts applied in the analysis. For each of the important samples cut out, we have checked that any reasonable varia-

tion of the cut would negligibly affect the result. As a final check, the fitted μ^+ lifetime from $B_\perp$ data is 2.205 ± 0.010 ± 0.040 μsec, consistent with the accepted value.

The $B_\perp$ data in Fig. 3(a) are fit to the radiatively corrected spectrum expected[14,15] for unpolarized μ^+ decay, smeared by a sum of gaussian resolution functions and by the expected e^+ energy-loss straggling. The fit simultaneously calibrates the edge position $x = 1$ and determines the momentum resolution and the (quadratic) dependence of the acceptance upon x.

In general, the $B_{||}$ spectrum in Fig. 3(b) can be represented as the shape expected from pure $(V-A)$ with $P_\mu = \cos\theta = 1$, in linear combination with the shape of the unpolarized spectrum in Fig. 3(a). The relative contribution of this small unpolarized fraction is essentially equal to $1-(\xi P_\mu \delta/\rho)\langle\cos\theta\rangle$. To fit this fraction, we use the $B_\perp$ fit to fix the x resolution and edge calibration, but allow the acceptance for $B_{||}$ data relative to that for $B_\perp$ data to vary linearly with x. This allows for the (<2%) difference in angular acceptance caused by the different field configurations near the target. Using the data with partly polarized μ^+ from π^+ decay in flight, we have checked that the $x = 1$ calibration is consistent for $B_{||}$ and $B_\perp$ fields. In the resulting curve in Fig. 3(b), the slight kink near $x = 1$ reflects the small fit unpolarized fraction, which arises mostly from the measured value $\langle\cos\theta\rangle = 0.9862$ for these data.

The limit on $\xi P_\mu \delta/\rho$ which we report here is based on this same fitting procedure carried out for data in each of five bins in $\cos\theta$. The subdivision provides a more precise measure of $\langle\cos\theta\rangle$ for each bin, and checks that the results of these fits are consistent with a linear dependence upon $\langle\cos\theta\rangle$. The fit values of $\xi P_\mu \delta/\rho$ for the four target materials are in satisfactory agreement (Table I).

A correction of +0.0012 ± 0.0005 has been made to all fit $\xi P_\mu \delta/\rho$, in order to account for misalignment of the μ^+ spin with respect to $\hat{p}_\mu$, due to Coulomb scattering upstream of the point at which $\hat{p}_\mu$ is measured. Table II summarizes the major sources of systematic error. All other sources contribute $\leq 10^{-4}$. In principle the systematic errors should not be correlated; in quadrature they add to ±0.0018. We have made no correction for unknown sources of μ^+ depolarization either along the beam or in the stopping target. Since such effects can only decrease the apparent result, we

therefore quote the limit

$$\xi P_\mu \delta/\rho > 0.9959 \quad (90\% \text{ confidence}).$$

The corresponding limits on the W_R mass and mixing parameters α and ζ are represented by the small bold contour in Fig. 1. In particular, for infinite W_R mass $|\zeta| < 0.045$ for any mixing angle $M(W_R) > 380$ GeV; and for zero mixing angle $M(W_R) > 450$ GeV.

The $B_\perp$ data can also be used for an independent μSR type measurement of ξP_μ. In Figure 4(a), 4(b) we show the measured time distributions of the data for all metal targets combined. The $B_\perp$ data are fit to the radiatively corrected decay rate assuming V-A values for the Michel parameters η, ρ, and δ. We perform a simultaneous maximum likelihood fit to 125,000 $B_\perp$ and 59,000 $B_{||}$ events.

For the $B_{||}$ case, the number of events is given by

$$N_{||}(t) = N_{||}^0 e^{-t/\tau_\mu} + BKD_{||}$$

In the $B_\perp$ case, the data are subdivided into four x bins, each 0.02 wide. The number of events in a given time interval, centered at t, after precession by $\rho = \omega t$, is

$$N_\perp(t) = N_\perp^0 \{\int_x A(x)dx + \langle \cos\theta \rangle_{t\ bin} \xi P_\mu \int_x B(x)dx\} e^{-t/\tau_\mu} + BKD_\perp$$

where

$$\langle \cos\theta \rangle_{t\ bin} = \frac{\int_{t-\Delta t}^{t+\Delta t} \langle \cos\theta(t' = \rho/\omega) \rangle e^{-(t'-t)/\tau_\mu} dt'}{\int_{t-\Delta t}^{t+\Delta t} e^{-(t'-t)/\tau_\mu} dt'} \cdot R(t)$$

and the effective relaxation function is

$$R(t) = \exp\{-2\sigma^2\tau_c^2[exp(-t/\tau_c) - 1 + t/\tau_c]\}$$

The thirteen fitted parameters are; ξP, the mean lifetime τ_μ, the precession frecuency ω, the relaxation parameters σ, τ_c, the time at the start of the of the first bin, the separate $B_\perp$ and $B_{||}$

backgrounds, and the acceptance dependent normalization for each x bin. A(x) and B(x) are calculated from equation (1). The results of the fit are shown superimposed on the $B_\perp$ data in Figure 5. The muon lifetime dependence has been divided out. The fitted value, corrected for the effects of the small constant background term, is $\xi P_\mu \delta/\rho = 0.9970 \pm 0.0038$ (statistical).

Again we must correct for the upstream Coulomb scattering ($+0.0012 \pm 0.0005$). For the $B_\perp$ data there is an additional correction for the possibility of a residual longitudinal magnetic field in the target region. We estimate that the uncertainties in the field cancellation correspond to a 0.0003 ± 0.0003 correction to $\xi P_\mu \delta/\rho$. We estimate the net systematic error to be 0.0014 and set a 90% confidence limit $\xi P_\mu \delta/\rho > 0.9918$. This limit is somewhat weaker than that obtained above using the $B_{||}$ data but it is still considerably more accurate than the previous world average. Although it is a more complex apparatus, this type of spectrometer clearly can be used for highly sensitive μSR measurements.

We are indebted to the entire TRIUMF management and staff for their splendid support of this experiment. In its early stages we benefited from discussion with J. Brewer, R. Cahn, K. Crowe, and W. Wenzel. Rapid commissioning of the polarimeter was made possible by the superb efforts of the LBL support staff. This research was supported in part by the U.S. Department of Energy, Division of Basic Energy Sciences, Office of Energy Research under contracts DE-AC03-76SF00098 and AC02-ER02289.

References

1. S. Weinberg, Phys. Rev. Lett. *19*, 1264 (1967); A. Salam, in Elementary Particle Theory, ed. N. Svastholm (Stockholm, 1968); S. Glashow, Nucl. Phys. *22*, 529 (1961).

2. J.C. Pati and A. Salam, Phys. Rev. *D11*, 566 and 2558 (1975); R.N. Mohapatra and J.C. Pati, Phys. Rev. *D12*, 1502 (1975).

3. M.A.B. Bég, R.V. Budny, R. Mohapatra, and A. Sirlin, Phys. Rev. Lett. *48*, 1252 (1977).

4. B.R. Holstein and S.B. Treiman, Phys. Rev. *D16*, 2369 (1977).

5. V.V. Akhmanov et al., Yad. Fiz. *6*, 316 (1967) (Sov. J. Nucl. Phys. *6*, 230 (1968)).

6. M. Bardon et al., Phys. Rev. Lett. *14*, 449 (1965).

7. J. Van Klinken, Nucl. Phys. *75*, 145 (1966).

8. J. Van Klinken et al., Phys. Rev. Lett. *50*, 94 (1983).

9. D. Schreiber and F.T. Calaprice, private communication; D. Schreiber, Ph.D. Thesis, Princeton University, 1983 (unpublished). We calculated the contour plotted in Fig. 1 using $A(0) = 0.0363 \pm 0.0008$; ft ratio $= 1.797 \pm 0.002$. See also F.T. Calaprice et al., Phys. Rev. Lett. *35*, 1566 (1975).

10. H. Abramowicz et al., [Phys. Lett., 1982].

11. G. Beall, M. Bander, and A. Soni, Phys. Rev. Lett. *48*, 848 (1982).

12. P. DeForcrand, Ph.D. Thesis, Univ. of Calif., Berkeley (1982), LBL-14692 (to be published).

13. J. Donoghue and B.R. Holstein, Phys. Lett. *113B*, 382 (1982).

14. F. Scheck, Phys. Lett. *C44*, 187 (1978).

15. A.M. Sachs and A. Sirlin, in *Muon Physics*, Vol. II, V. Hughes and C.S. Wu, eds. (Academic Press, N.Y., 1975), p. 50.

16. A.E. Pifer, T. Bowen, and K.R. Kendall, Nucl. Inst. Meth. *135*, 39 (1976).

17. C.J. Oram, J.B. Warren, G.M. Marshall, and J. Doornbos, Nucl. Inst. Meth. *179*, 95 (1981).

18. K. Halbach, private communication.

TABLE I. Results of fits to $\xi P_\mu \delta/\rho$ for μ^+ stopping in each of four target foils, and for the combined sample. Errors are statistical.

Target	Thickness (mg/cm^2)	$\xi P_\mu \delta/\rho$
Al	154.5	$0.9978\ ^{+0.0028}_{-0.0028}$
Cu	233.4	$1.0026\ ^{+0.0029}_{-0.0026}$
Ag	275.1	$0.9994\ ^{+0.0036}_{-0.0031}$
Au	232.6	$0.9970\ ^{+0.0035}_{-0.0034}$
Total	—	$0.9989\ ^{+0.0015}_{-0.0015}$

TABLE II. Major sources of systematic error and their estimated contributions.

Source of systematic error	Error
Upstream Coulomb scattering of μ^+	± 0.0005
Correction of θ_μ and θ_e for bending in $B_{\|\|}$ field at target	± 0.0010
Smearing of θ_μ and θ_e due to measurement error and scattering	± 0.0006
Possible shift in θ_e due to random hits and inefficiencies in D1 and D2	± 0.0005
Method of averaging $\langle \cos\theta \rangle$	± 0.0004
Difference in $x=1$ edge calibration between $B_\perp$ and $B_{\|\|}$ data	± 0.0008
Normalization of $B_{\|\|}$ data with respect to $B_\perp$ data	± 0.0007

Figure Captions

FIG. 1. Experimental 90%-confidence limits on the $W_{L,R}$ mass-squared ratio α and mixing angle ζ describing possible right-handed charged currents. Muon-decay contours are derived from decay rate measurements at the spectrum endpoint (bold, this experiment); the polarization parameter ξP_μ (dotted, Ref. 5); and the Michel parameter ρ (solid, Ref. 6). Nuclear β decay contours are obtained from the Gamow-Teller β polarization (dot-dashed, Ref. 7); the comparison of Gamow-Teller and Fermi β polarizations (long-dashed, Ref. 8); and the ^{19}Ne asymmetry $A(0)$ and ft ratio, assuming CVC (short-dashed, Ref. 9). Limits from the y distributions in νN and $\bar{\nu} N$ scattering (double lines, Ref. 10) are valid irrespective of the ν_R mass. One experiment (dotted contour) is marginally inconsistent with $\alpha = \zeta = 0$ at the 90% confidence interval; for clarity, the corresponding inner contour is suppressed.

FIG. 2. Plan view of muon polarimeter at TRIUMF. "Surface" μ^+ are incident from the top. After crossing proportional wire chambers P1 and P2 and scintillator S1, the muons stop in a foil target within the uniform region of a 1.1-T spin-holding longitudinal field, or alternately a 70-gauss spin-precessing field. After registration in P3, S2, and driftchambers D1 and D2, the decay positron is focussed by the solenoidal field lens between D2 and D3, and analyzed by the 98° horizontally focussing spectrometer consisting of D3, D4, and the cylindrical dipole magnet. The trigger is $T1 \cdot T2$, where $T1$ is $P1 \cdot S1 \cdot P2 \cdot \bar{V}1 \cdot \bar{P}3 \cdot \bar{S}2 \cdot \bar{V}2$ at the μ^+ stopping time, $T2$ is $P3 \cdot S2 \cdot S3 \cdot \bar{P}1 \cdot \bar{S}1 \cdot \bar{V}1 \cdot \bar{P}2 \cdot \bar{V}2$ at the μ^+ decay time, and $V1$ and $V2$ are veto scintillators surrounding $S1$ and $S2$, respectively (not shown).

FIG. 3. Distributions in the ratio of the positron momentum to its maximum value: (a) with the μ^+ spin $\vec{s}$ precessed about an axis transverse to the direction $\hat{p}_e$ of positron emission; (b) with $\vec{s}$ held so that $2\langle \vec{s} \cdot \hat{p}_e \rangle = 0.9850$. The horizontal scale is calibrated by the edge position in (a). Distributions are uncorrected for acceptance; errors are statistical. The solid line in (a) is a fit with parameters which are empirical except at the shoulder; the gaussian part of the resolution is <0.2% rms. The fit in (b) is to a linear combination of the shape of (a) with that expected from pure $(V-A)$ and 100% μ^+ polarization opposite to $\hat{p}_e$.

FIG. 4. (a) Time distribution of positrons for $B_{||}$ data, (b) Time distribution of positrons for $B_{\perp}$ data. In both cases the events are binned in 0.079 μsec intervals. The solid lines correspond to the fit described in the text.

FIG. 5. Time distribution of positrons for $B_{\perp}$ data with fitted lifetime divided out. The solid histogram corresponds to the fit described in the text.

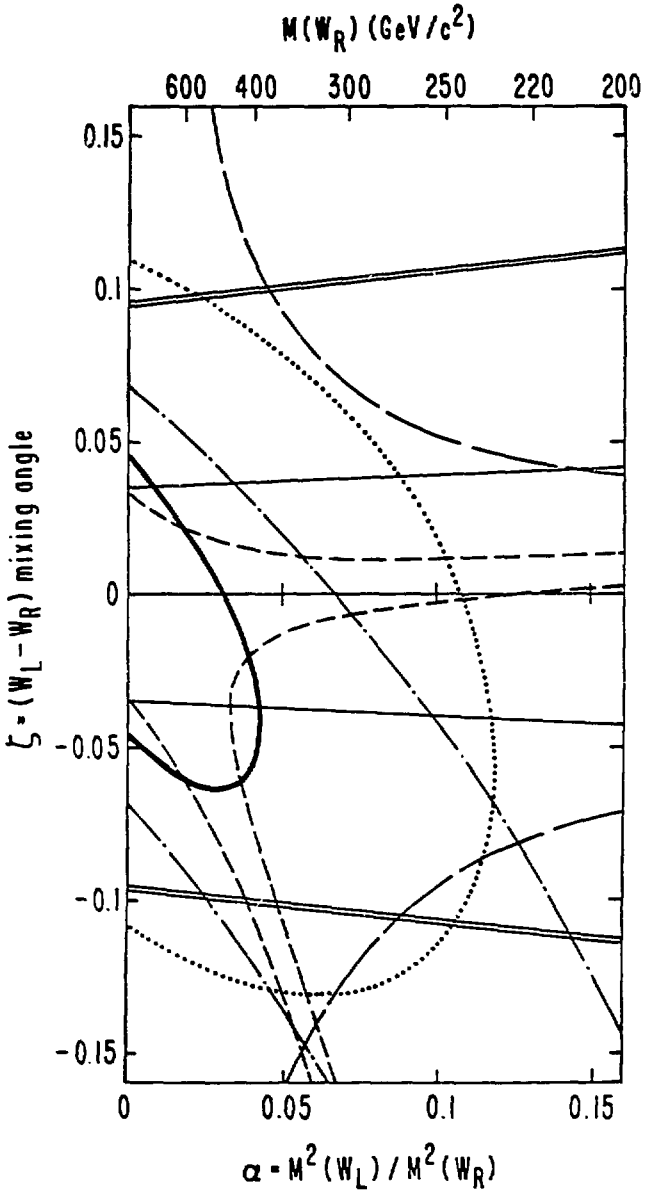

FIG. 1

XBL 834-145

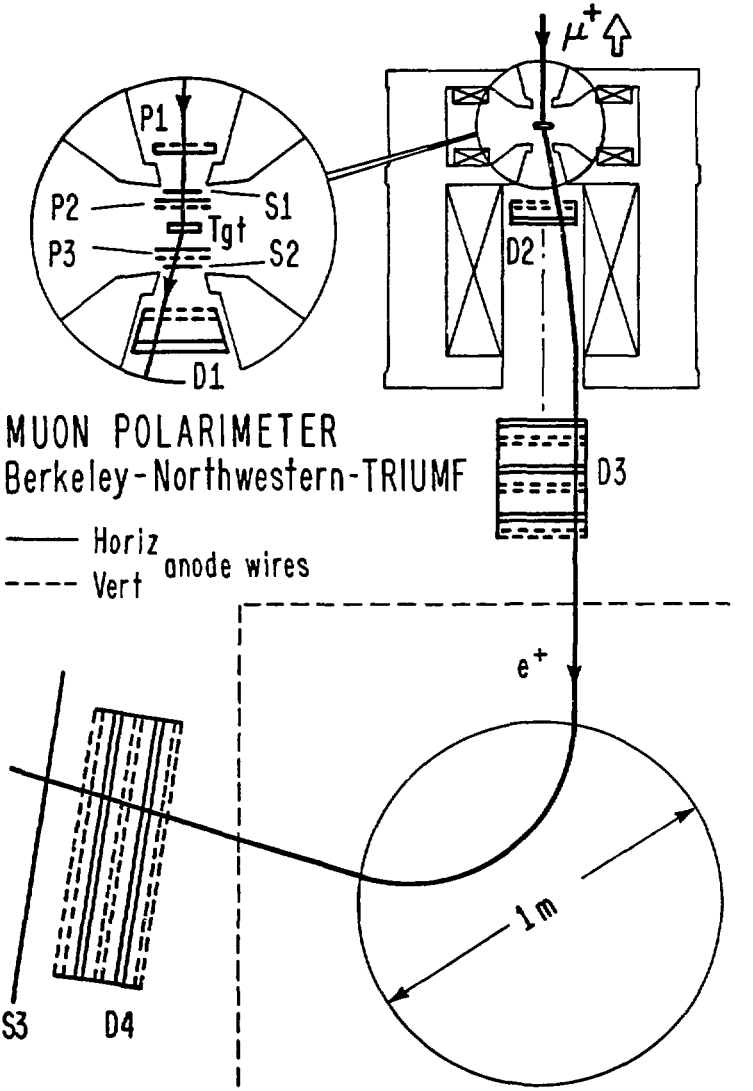

FIG. 2

XBL 834-147

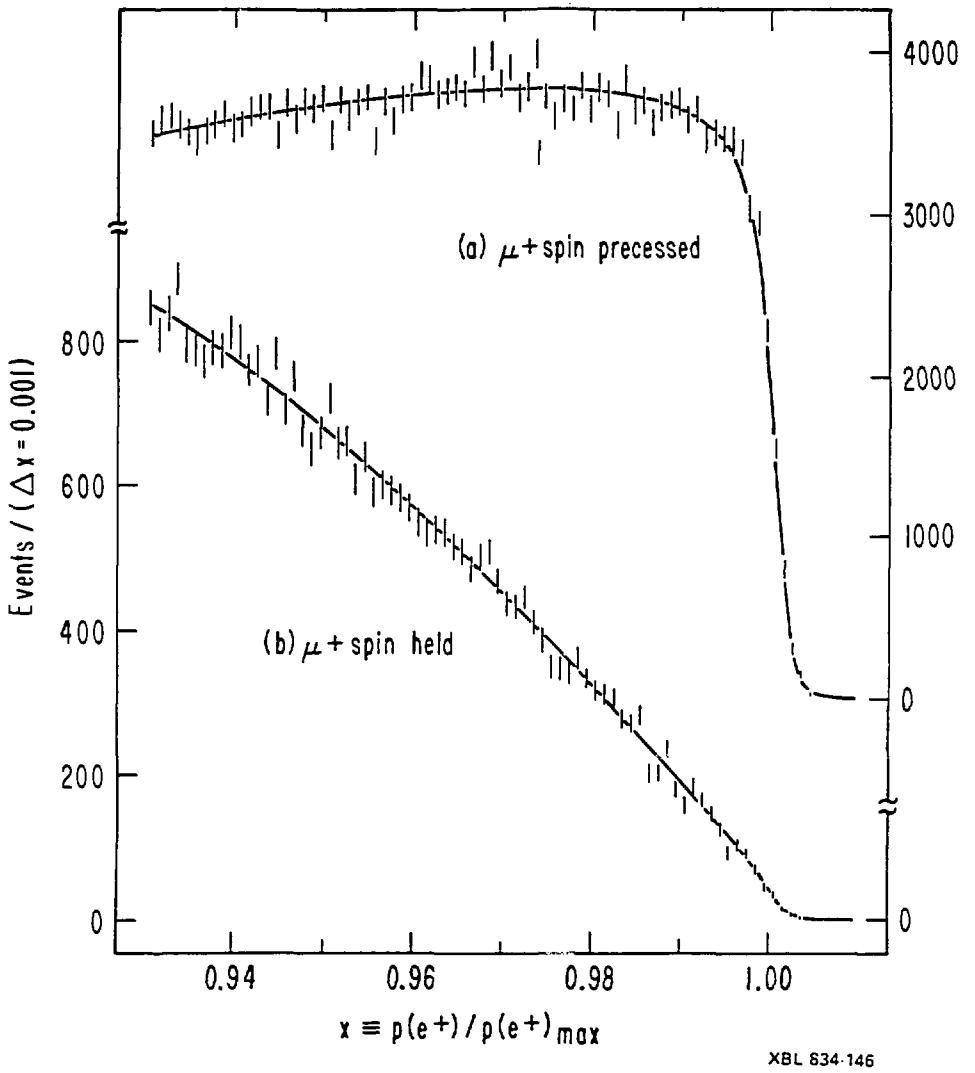
(a) μ+ spin precessed
(b) μ+ spin held
Events / (Δx = 0.001)
x ≡ p(e+) / p(e+)max
0.94
0.96
0.98
1.00
0
200
400
600
800
1000
2000
3000
4000
XBL 834-146

FIG. 3

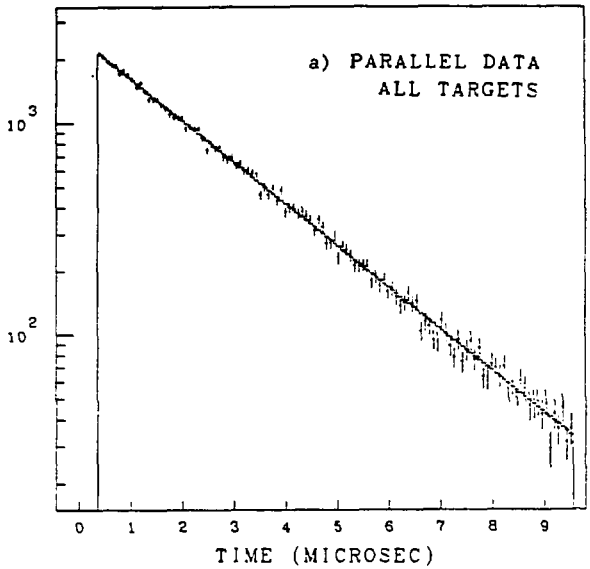
a) PARALLEL DATA
ALL TARGETS
10^3
10^2
0 1 2 3 4 5 6 7 8 9
TIME (MICROSEC)

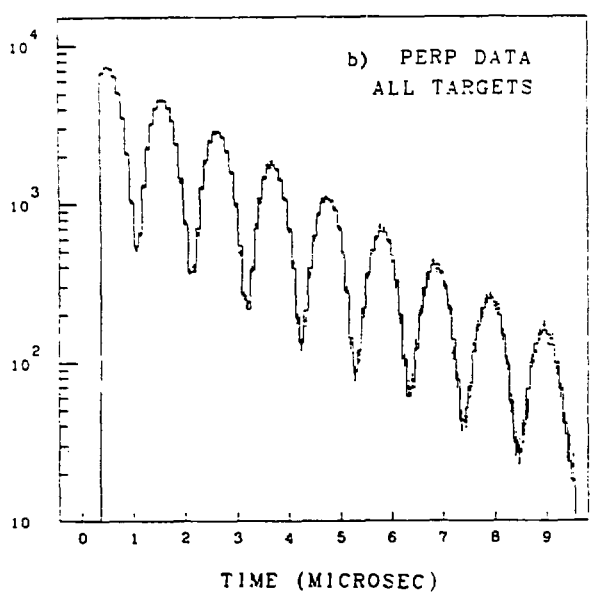
b) PERP DATA
ALL TARGETS
10^4
10^3
10^2
10
0 1 2 3 4 5 6 7 8 9
TIME (MICROSEC)

FIG. 4

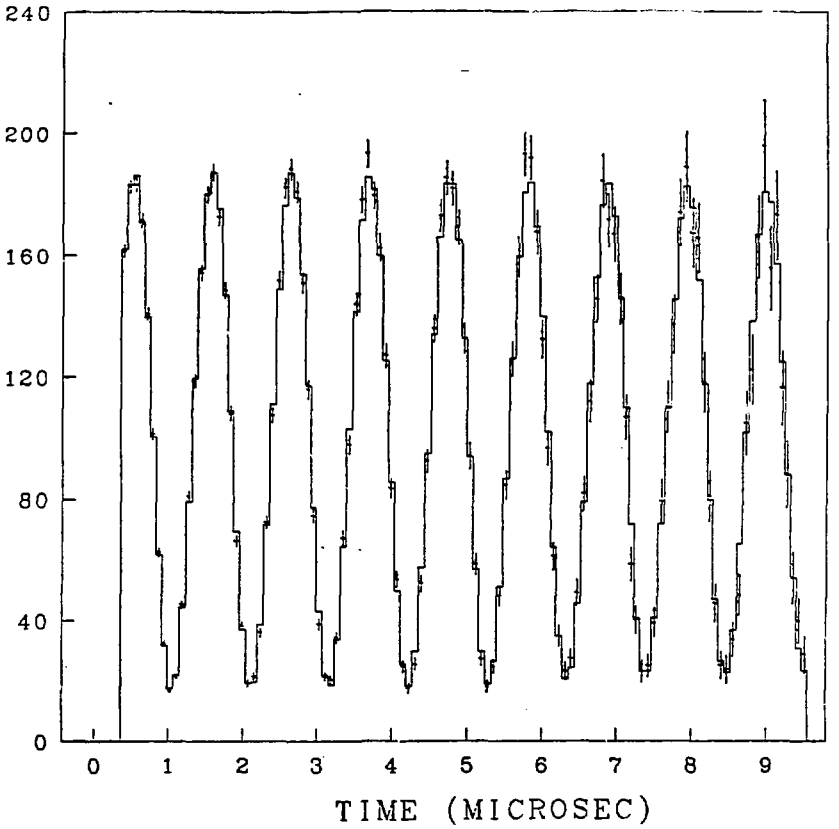

FIG. 5